SC-DR-66-2667

January 1967

AEROSPACE NUCLEAR SAFETY

STRESS ANALYSIS OF THE SNAP-27 LUNAR FLIGHT CASK

R. E. Davis, 1511
R. L. Dineen, 1542
R. E. Berry, 9312

565 7000

MASTER

SPECIFIED DISTRIBUTION ONLY

SANDIA LABORATORIES

OPERATED FOR THE U. S. ATOMIC ENERGY COMMISSION BY SANDIA CORPORATION | ALBUQUERQUE, NEW MEXICO; LIVERMORE, CALIFORNIA

DISCLAIMER

SPECIFIED DISTRIBUTION ONLY

(31)

SC-DR-66-2667

STRESS ANALYSIS OF THE SNAP-27 LUNAR FLIGHT CASK

R. E. Davis, 1511
R. L. Dineen, 1542
R. E. Berry, 9312
Sandia Laboratory, Albuquerque

Approved by: V. E. Blake
V. E. Blake, 9310

MASTER

ABSTRACT

A stress analysis was performed on the beryllium lunar flight cask to determine if structural failure of the cask will occur during reentry after an Apollo mission abort. The analysis indicates that failure will not occur during reentry from an earth orbit abort; failure will probably occur after a lunar transfer orbit abort if the trajectory angle is near -6.4 degrees, and will occur if the angle is near -30 degrees.

January 1967

%%%

SUMMARY

A stress analysis was performed on the beryllium lunar flight cask (LFC) to determine whether or not the LFC will return the fuel capsule assembly (FCA) intact following an Apollo mission abort. The analysis established that the LFC will return the FCA intact after an earth orbit abort. There is a low probability that the LFC will return the FCA intact after a lunar transfer orbit abort when the reentry angle is near -6.4 degrees; the LFC will not reenter the FCA intact after a lunar transfer orbit abort when the reentry angle is near -30 degrees.

Because of the numerous unknowns in the trajectories, heating rates, and material properties, only the following conditions were analyzed: (1) nominal, (2) 20 percent above nominal, and (3) 20 percent below nominal.

TABLE OF CONTENTS

STRESS ANALYSIS OF THE SNAP-27 LUNAR FLIGHT CASK

Introduction

The SNAP-27 radioisotope thermoelectric generator (RTG) provides the electric power for the Apollo lunar surface experiment package (ALSEP). To provide a cold system for emplacement of the experiments on the lunar surface and to provide the greatest probability of returning the radioisotope fuel to earth in the event of a mission abort, the radioisotope fuel is packaged independently of the remainder of the ALSEP.

The fuel capsule assembly (FCA) is placed in the lunar flight cask (LFC) for the trip to the lunar surface. The LFC is mounted on an exterior surface of the lunar module (LM) to provide maximum probability that the LFC will be released from the LM at the time of abort or shortly after reentry into the earth's atmosphere begins. The early release of the LFC is necessary to allow a free-flight reentry and, thereby, intact reentry of the radioactive fuel within the fuel capsule assembly.

The LFC is designed as a reentry body; it incorporates ablative material on the nose and aft flare, and has a beryllium barrel to dissipate the heat which results from the radioactive decay of the fuel material. Because the barrel is a metallic structure sensitive to heat, the design criteria established to indicate failure were based on the beryllium properties.

This structural analysis was performed to determine if structural failure will occur during reentry and if so, the approximate time and altitude at which the FCA will be released from the LFC. The structural analysis of the LFC was performed in conjunction with an aerothermodynamic analysis. The results of the aerothermodynamic analysis are reported in Reference 1.

Trajectories Examined

To determine the structural adequacy of the LFC, typical reentry trajectories were chosen for analysis. The trajectories examined were earth orbital decay, a -6.4 degree reentry, and a -30 degree reentry. In all three cases, the LFC was assumed to have an angle of attack of 179 degrees with a pitch rate of 5.74 degrees per second.

Reentry of the vehicle in the first case was assumed to occur at an altitude of 400,000 feet; this represents the condition for a 100-nm parking orbit. The other two trajectories represent probable supercircular velocity reentry conditions. Two possibilities were examined: separation of the LM from the command service module (CSM) after midcourse corrections were made, and separation of the LM from the CSM before midcourse corrections were made. A reentry angle of -6.4 degrees is representative of the first case, while -30 degrees applies to the second case.

Method of Analysis

Assumptions

The LFC (Figure 1) consists essentially of two end caps covered with an ablative material and connected by a beryllium cylinder (the centerbody). The aft end of the fuel capsule assembly is attached to a bulkhead of the LFC end cap, while the forward end of the FCA is restrained in the lateral direction only.

The ablative material on the two caps effectively insulates these parts of the structure, and high temperatures will not occur in these regions. The centerbody is not insulated and will experience high temperatures. This section of the structure can also be expected to sustain large bending moments as well as axial loads. In the analysis, then, attention was confined to the centerbody.

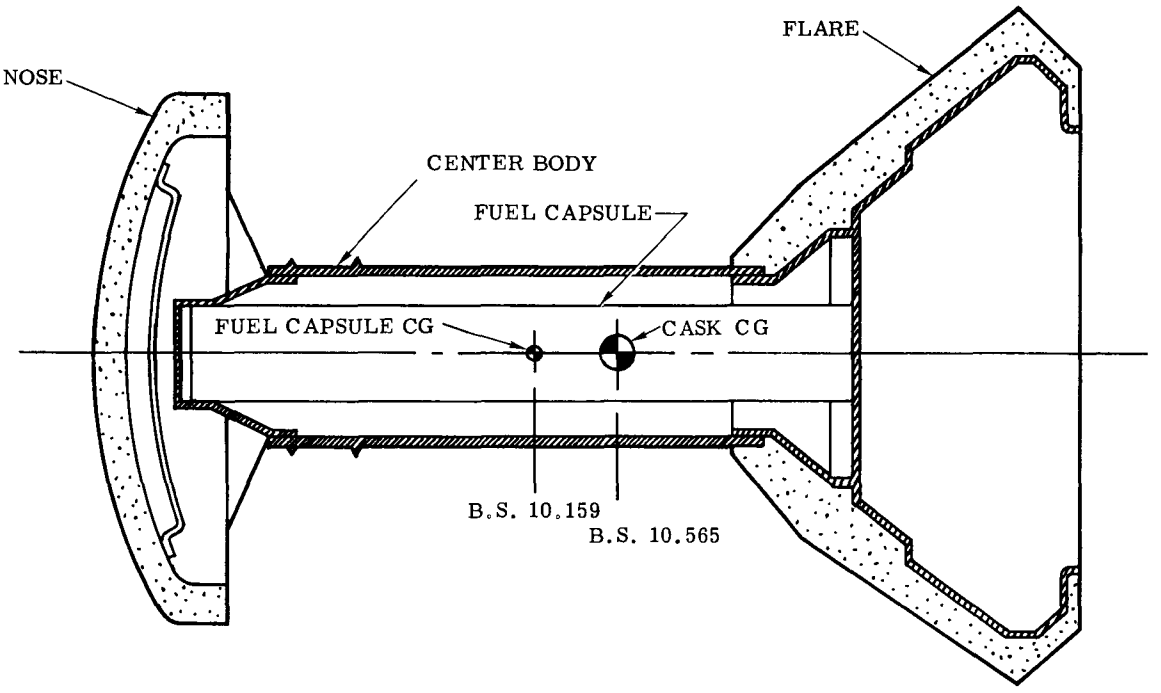

LUNAR FLIGHT CASK	
Wt	21.732 lb
CG	10.565 in.
MI	938 lb-in.^{2}

FUEL CAPSULE ASSEMBLY	
Wt	14.345 lb
CG	10.159 in.
MI	314.437 lb-in.^{2}

Figure 1. Cross section of lunar flight cask

Failure Criteria

The most obvious effect of temperature would be melting of the beryllium; this condition, then, was one criterion for failure. For situations where the temperature is below the melting point of the material, yielding of the beryllium was taken as the failure criterion. In the temperature range considered, i.e., temperatures very near the melting point, any yielding in the material would most certainly provide a lower limit on the structural capability of the centerbody. At the very least, it would be the prelude to the formation of a plastic hinge in the structure. Yielding of the material, then, was the other criterion adopted for failure.

The relationship between temperature and yield strength for beryllium was obtained from Reference 2. Unfortunately, data are not available for the yield stress between 2060°R and the melting point, 2800°R. A straight-line interpolation was assumed between these two points. This represents, most probably, a conservative estimate, since one might expect the strength to approach the melting point asymptotically and thereby be below the straight-line interpolation.

Temperature Data

The initial step in the analysis was to determine the temperature of the fuel capsule assembly as a function of time and altitude. This part of the problem was handled by Sandia Division 9314 using a computer program they developed which predicts the thermal response of the assembly to a reentry environment. The aerodynamic heating rates used were based on Cornell Aeronautical Laboratory shock data for the predicted angles of attack. To compensate for inaccuracies in the data and the method of analysis, +20 and -20 percent heating rates were included along with the nominal value.

The node points on the centerbody for which temperatures were obtained are shown in Figure 2. Points 4, 5, 6, and 7 experienced the highest temperatures. They also would be subject to the largest loading. Therefore, the analysis was further limited to these four nodes. Figures 3 through 9 give the resultant temperatures as a function of time for each of these nodes.

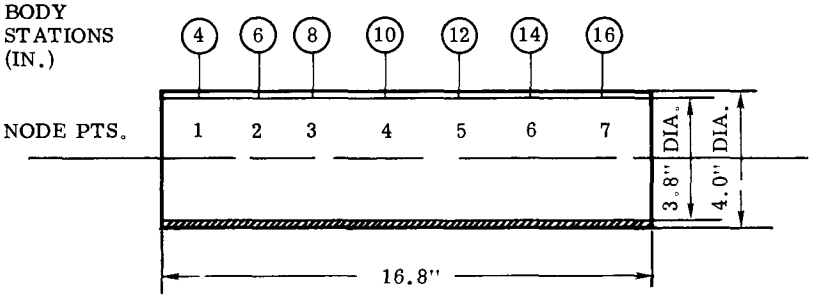

Figure 2. Node points on beryllium centerbody

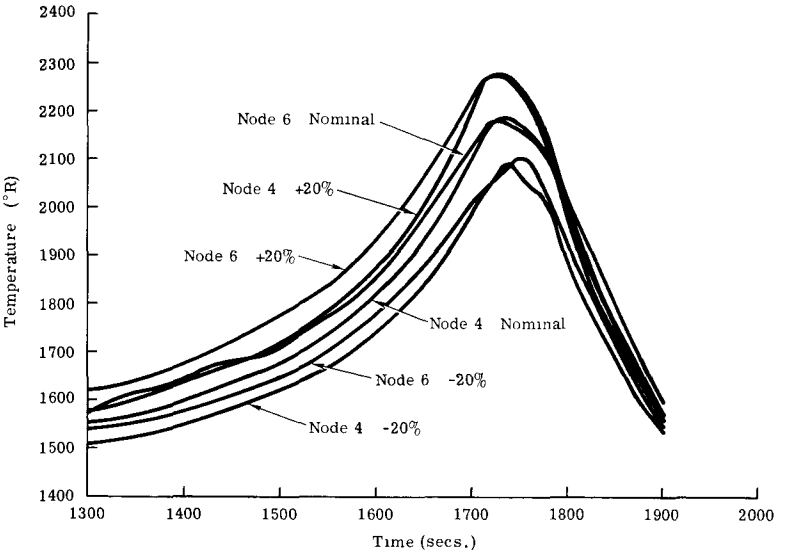

Figure 3. Temperature-time curves for the orbital decay condition at Nodes 4 and 6

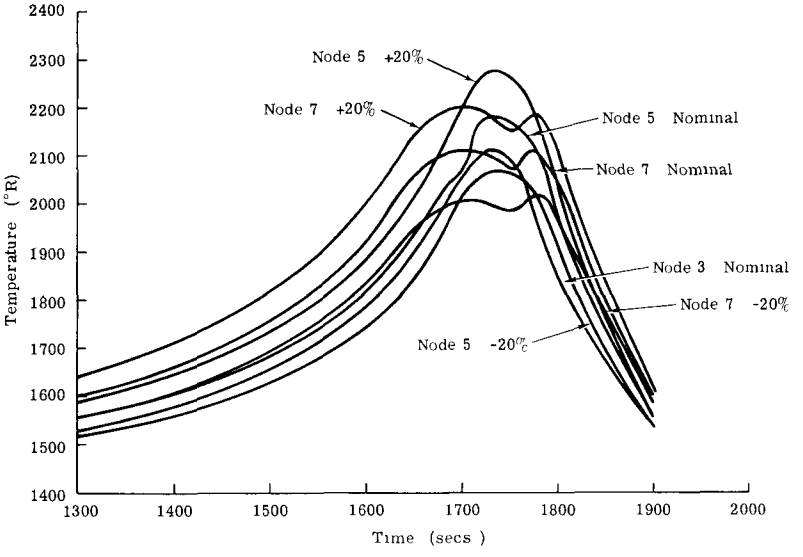

Figure 4. Temperature-time curves for the orbital decay condition at Nodes 5 and 7

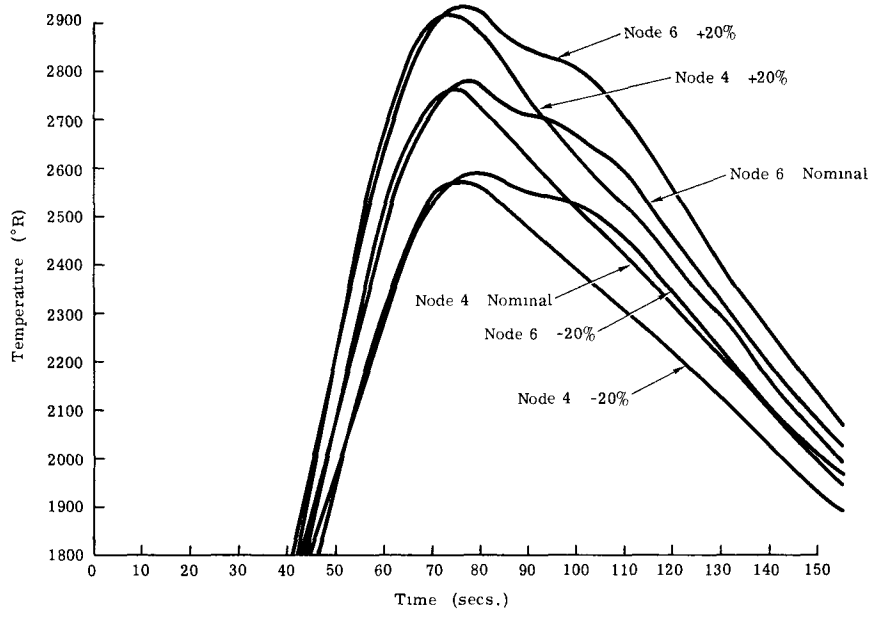

Figure 5. Temperature-time curves for the -6.4 degree reentry condition at Nodes 4 and 6

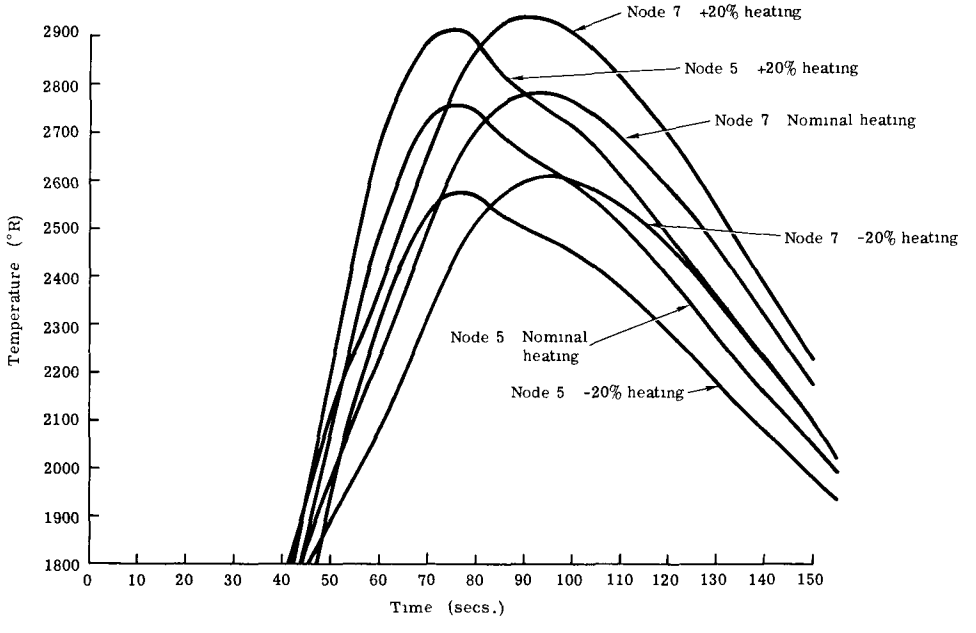

Figure 6. Temperature-time curves for the -6.4 degree reentry condition at Nodes 5 and 7

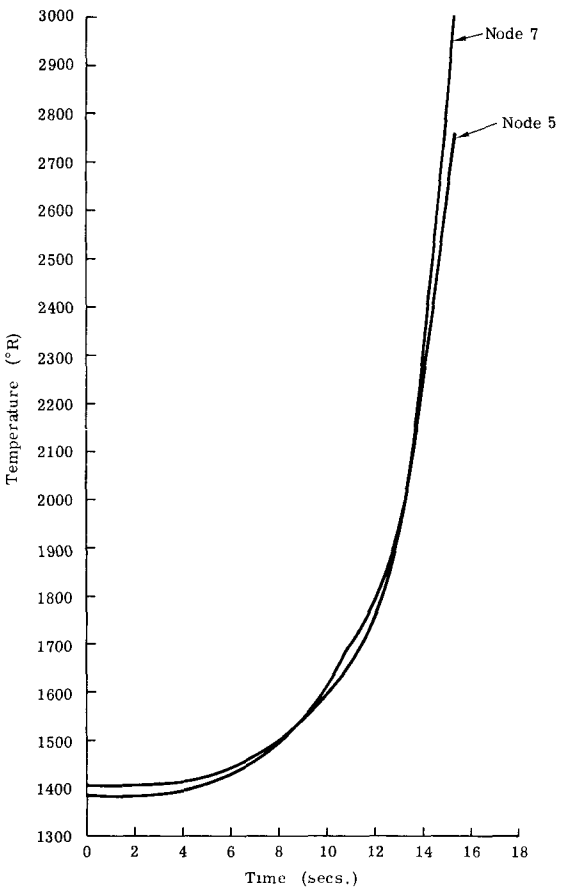

Figure 7. Temperature-time curves for the -30 degree re-entry condition at Nodes 5 and 7 (-20% heating rate)

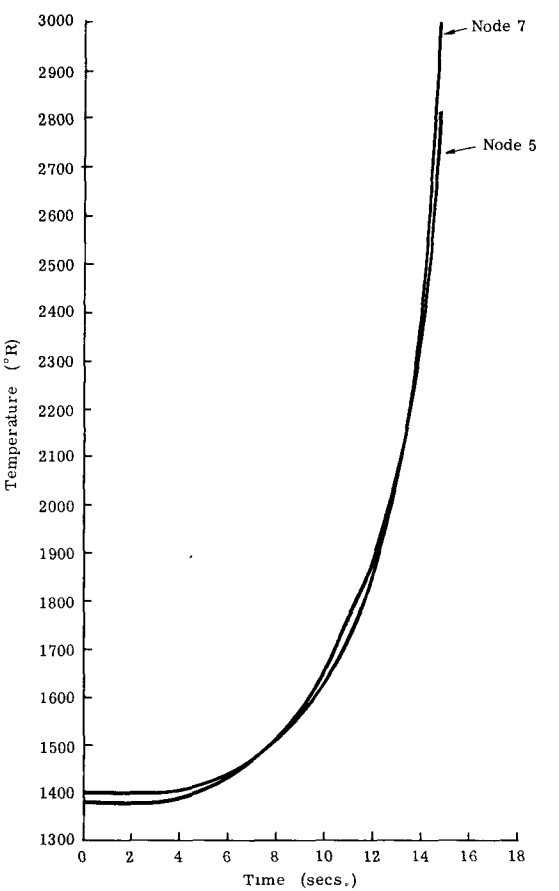

Figure 8. Temperature-time curves for the -30 degree re-entry condition at Nodes 5 and 7 (nominal heating rate)

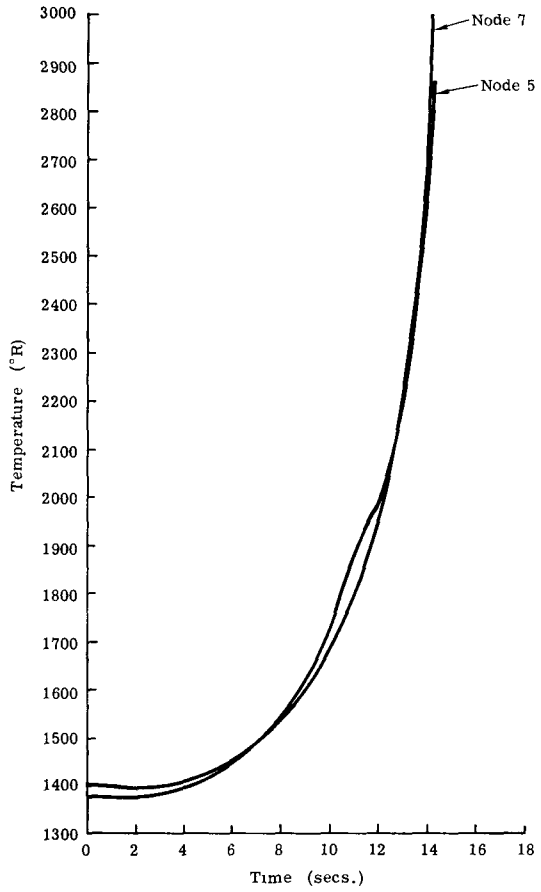

Figure 9.

Temperature-time curves for the -30 degree reentry condition at Nodes 5 and 7 (+20% heating rate)

For the orbital decay condition, the maximum temperature occurs at about 1725 seconds. The time interval between 1650 and 1820 seconds was chosen for investigation. Table I indicates the temperature corresponding to the actual times used.

The same procedure was followed for the -6.4 degree reentry condition. Table II gives the temperatures used for this trajectory. Even though the melting point temperature is exceeded for Node 7, times were examined beyond this point to establish the shape of the stress-temperature curve.

TABLE I

Temperatures for the Orbital Decay Condition

Node / Time	-20%				Nominal				+20%			
	4	5	6	7	4	5	6	7	4	5	6	7
1650	1840	1845	1885	1950	1935	1935	1985	2060	2010	2020	2070	2150
1700	1995	2010	2015	2005	2100	2070	2130	2110	2220	2210	2230	2200
1725	2070	2065	2060	2000	2180	2180	2180	2100	2280	2275	2280	2185
1750	2065	2065	2105	1985	2170	2170	2160	2075	2250	2260	2245	2150
1770	2030	2040	2060	2010	2130	2135	2130	2115	2180	2210	2170	2185
1780	1990	2010	2010	2020	2090	2095	2100	2110	2130	2165	2110	2190
1800	1890	1905	1920	1965	1970	1970	1990	2040	2000	2025	2010	2100
1820	1790	1810	1830	1885	1850	1870	1890	1950	1890	1900	1925	1995

NOTE: Temperatures are in degrees Rankine.

TABLE II

Temperatures for the -6.4 Degree Reentry Condition

		Time (sec)								
		50	55	58	63	66	70	75	77	80
Node 4	-20%	1940	2125	2225	2390	2470	2540	2570	2570	2560
	Nom.	2070	2300	2430	2610	2660	2730	2760	2750	2730
	+20%	2200	2460	2600	2750	2830	2900	2920	2900	2880
Node 5	-20%	1960	2150	2250	2380	2450	2530	2570	2580	2570
	Nom.	2060	2290	2420	2580	2650	2720	2755	2750	2740
	+20%	2190	2430	2600	2750	2820	2895	2910	2905	2890
Node 6	-20%	1960	2130	2220	2370	2450	2520	2580	2585	2590
	Nom.	2080	2290	2390	2560	2640	2720	2770	2780	2770
	+20%	2210	2440	2550	2715	2815	2885	2930	2930	2920
Node 7	-20%	1880	1980	2040	2140	2210	2315	2425	2460	2510
	Nom.	1970	2110	2180	2300	2370	2490	2610	2650	2700
	+20%	2100	2240	2320	2450	2540	2655	2780	2820	2870

NOTE: Temperatures are in degrees Rankine.

The -30 degree reentry trajectory exhibited an extremely high temperature at very early times. Preliminary investigation of these stress-temperature conditions indicated structural failure very early in the reentry phase. Consequently, a more detailed analysis was not warranted, and the remainder of the analysis was confined to the orbital decay and -6.4 degree reentry conditions.

External Loads

With the times in each trajectory chosen, the resultant loads acting on the assembly were calculated by Division 9314. Starting with a given time, the altitude and velocity were obtained from the previously determined trajectory. The value of the dynamic air pressure, q, was calculated using the relationship

$$q = \frac{\rho v^2}{2g} = \frac{\rho v^2}{64.4}$$

where

ρ = density of air at a given altitude, pounds/ft^3;
v = velocity at the same altitude, fps; and
g = acceleration due to gravity, ft/sec^2.

The absolute value of the maximum angle of attack was obtained from a curve which relates this parameter to altitude (Reference 3).

The force coefficients were obtained from curves previously determined by Division 9314 which relate these coefficients to the angle of attack. Finally, the resultant normal and axial loads, as well as the resultant moment, were obtained from the equations:

$N = C_n qS$ (normal force, lb),
$A = C_A qS$ (axial force, lb), and
$M = C_M qS\ell$ (moment, in.-lb).

The values of "S" and "ℓ" used in these equations were 0.087 and 0.333, respectively (Reference 3). Tables III and IV give the values of these forces for the times in Tables I and II.

TABLE III

Distribution of External Loads
on the Fuel Cask for the Orbital Decay Condition

①	②	③	④	⑤	⑥	⑦	⑧	⑨	⑩	⑪
Time	N	A	M	0.51805 x ②	0.05 x ④	P_1 = ⑤ - ⑥	P_{21} = ② - ⑦	P_F = 0.833 x ③	P_A = ③ - ⑨	$P_{18.5}$ = 0.645 x ③
1650	19.2	13.8	85.2	9.95	4.3	5.7	13.5	12.0	2.0	9.0
1700	24.3	40.3	187.2	12.6	9.4	3.2	21.1	33.6	6.7	26.0
1725	44.4	72.0	312.0	23.0	15.6	7.4	37.0	60.0	12.0	46.0
1750	48.0	114.0	427.8	24.9	21.4	3.5	44.5	95.0	19.0	74.0
1770	38.6	158.0	200.4	20.0	10.0	10.0	28.6	131.6	26.4	101.9
1780	41.3	169.8	214.8	21.4	10.7	10.7	30.6	141.4	28.4	109.5
1800	30.75	117.0	152.2	15.9	7.6	8.3	22.5	97.0	20.0	75.0
1820	22.3	66.8	155.2	11.6	7.8	3.8	18.5	56.0	11.0	43.0

P_1, P_{21}, P_A, P_F are applied air loads.

$P_{18.5}$ - Axial force exerted by fuel rod.

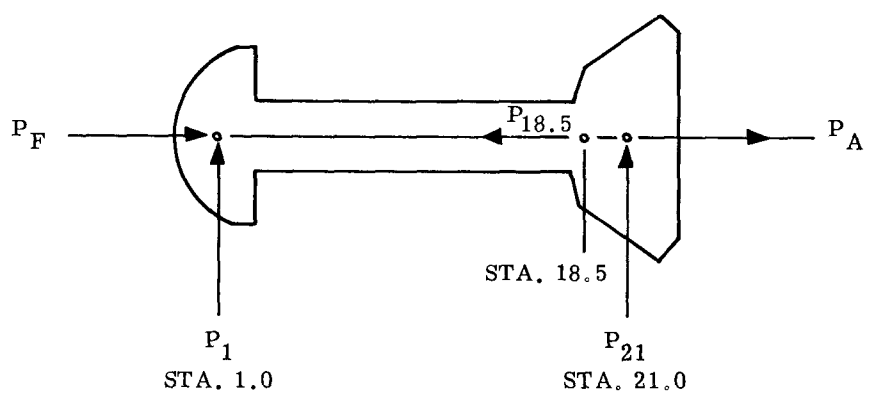

TABLE IV

Distribution of External Loads
on the Fuel Cask for the -6.4 Degree Reentry Condition

Time (sec)	N (lb)	A (lb)	M (in.-lb)	① 0.5217 N (lb)	② 0.05 M (lb)	P_1 = ① - ② (lb)	P_{21} = N - P_1 (lb)	P_F = 0.833 A (lb)	P_A = A - P_F (lb)	$P_{18.5}$ = 0.660(A) (lb)
50	20.34	61.41	122.64	10.61	6.13	4.48	15.86	51.15	10.26	40.5
55	26.51	96.40	125.16	13.83	6.26	7.57	18.94	80.30	16.10	63.6
58	27.28	121.24	109.02	14.23	5.45	8.78	18.50	100.99	20.25	79.9
63	33.6	168.0	117.84	17.53	5.89	11.64	21.96	139.94	28.06	111
66	38.8	194.0	126.00	20.24	6.30	13.94	24.86	161.60	32.40	128.2
70	47.2	236.0	153.60	24.62	7.68	16.94	30.26	196.59	39.41	156
75	56.0	280.0	153.60	29.22	7.68	21.54	34.46	233.24	46.76	185
77	59.0	295.0	162.00	30.78	8.10	22.68	36.32	245.74	49.26	195
80	60.6	304.0	166.80	31.62	8.34	23.28	37.32	253.23	50.77	201

To determine the resultant stresses at the various node points on the centerbody, these loads were distributed over the fuel cask to permit calculation of shears, moments, and axial loads. Using wind-tunnel data, Division 9314 concluded that 5/6 of the axial force should be applied to the nose and the remainder to the flare. These forces were taken to act at Body Stations 1 and 21 and were designated P_F and P_A, respectively.

The normal (or lateral) force was assumed to act in two parts: again at BS 1 and at BS 21. The two loads were proportioned to give a moment equal to the resultant externally applied moment. The derivation for these two forces was as follows.

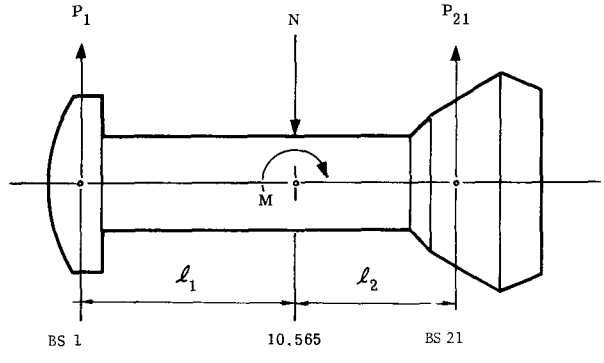

$$\Sigma F_{normal} = N$$
$$P_1 + P_{21} = N \qquad (1)$$
$$\therefore \quad P_{21} = N - P_1$$

$$\Sigma M_{CG} = M$$
$$P_{21}\ell_2 - P_1\ell_1 = M \qquad (2)$$

Substituting from Eq. (1) into Eq. (2),

$$(N - P_1)\ell_2 - P_1\ell_1 = M$$

$$N\ell_2 - P_1\ell_2 - P_1\ell_1 = M$$

$$P_1(\ell_1 + \ell_2) = N\ell_2 - M$$

$$P_1 = \frac{N\ell_2 - M}{\ell_1 + \ell_2},$$

where

$$\ell_1 = 10.565 - 1 = 9.565 \text{ in.}$$

$$\ell_2 = 21 - 10.565 = 10.435 \text{ in.}$$

$$\ell_1 + \ell_2 = 20 \text{ in.}$$

$$\therefore P_1 = \frac{10.435N - M}{20} = 0.5217N - 0.05M.$$

Tables III and IV are a summary of these calculations for the orbital decay and the -6.4 degree reentry trajectories.

Shears, Moments, and Axial Loads

Calculation of the shear, moment, and axial load at each node point due to the applied loads and the inertial effects was performed using a computer program developed by Sandia Division 2223. The fuel cask assembly was digitized for this program by Section 2211-5. Two programs were run for each set of applied loads. In the first program, all the items of the fuel cask were included. The results of this run provided the values of the shears and moments for the capsule-cask combination. Since the fuel capsule is connected to the fuel cask at its aft end only, it had to be removed and an axial load inserted to simulate the inertial effect of the rod to determine the axial load in the cask at body stations forward of this connection. The output of these two programs included the shear, moment, and axial load at even-numbered body stations, as well as the resultant lateral, axial, and angular accelerations of the entire unit due to the applied loads.

Corrections were then made to the moments calculated in the first computer run to account for the effects of the forward lateral support on the fuel capsule. Because of its relatively flexible connection, the capsule was considered to be simply supported on both ends. The lateral acceleration of the fuel capsule was calculated using the following procedure.

$$N_Y' = N_Y - \frac{\ddot{\alpha}\,\bar{x}}{g},$$

where

N_Y is the lateral acceleration of the CG of the fuel cask assembly as obtained from the computer program (g),

$\ddot{\alpha}$ is the angular acceleration of the complete unit (rad/sec^2), and

$\bar{x}$ is the difference between the CG of the assembly and the fuel rod (in.).

$$\bar{x} = 10.565 - 10.159 = 0.406 \text{ in.}$$

$$\therefore N_Y' = N_Y - \frac{0.406}{386}\ddot{\alpha}$$

$$= N_Y - 0.001052\,\ddot{\alpha}$$

The forward reaction R_F may be calculated from the expression,

$$R_F = N_Y' \frac{W}{2} - \frac{\ddot{\alpha} I}{16.8}; \text{ but}$$

$$W = 14.345 \text{ lb and}$$

$$I = \frac{314.437}{386} = 0.8146 \text{ lb-in.-sec}^2.$$

$$\therefore R_F = 7.1725\, N_Y' - 0.04849\,\ddot{\alpha} \text{ and}$$

$$R_A = N_Y' W - R_F.$$

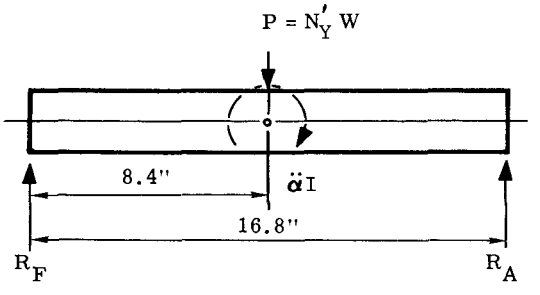

The final value for the resultant moment in the beryllium centerbody at a node point (designated as Section A-A on the diagram below) was obtained by subtracting from the moment due to P_1 the moment due to R_F, i.e.,

$$M_{resultant} = P_1 \ell - R_F \ell'$$

$$= M_1 - M_N.$$

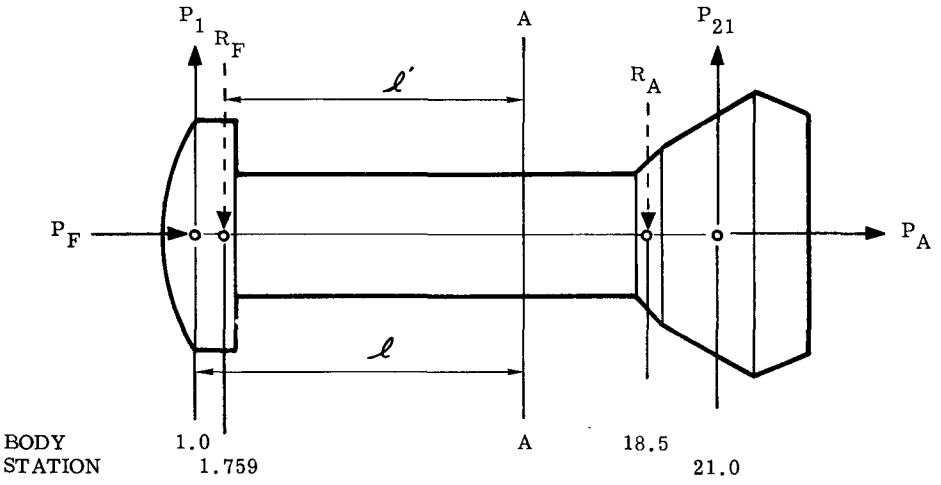

Tables V and VI list the moments due to the external loads on the complete flight cask, while Tables VII and VIII list the resultant moments.

The stress due to the moment at each node point was calculated using the formula for bending stress and the section properties of the beryllium centerbody.

$$I = \frac{\pi}{4}\left(r_1^4 - r^4\right)$$

where

$r_1 = 2$ in.

$r = 1.9$ in.

$I = 0.785\ (16 - 13.032) = 2.336$ in.^{4}

$C = 4/2 = 2$ in.

$\therefore$ the section modulus for the centerbody is:

$$S = \frac{I}{c} = 1.168 \text{ in.}^3 \text{ and}$$

$$\sigma_{bending} = \pm \frac{M_R}{S} = 0.856\ M_R \text{ (psi)}.$$

The axial stress was calculated by dividing the axial load at the node point by the cross-sectional area of the centerbody.

$$A = \pi\left(r_1^2 - r^2\right)$$

where

$r_1^2 = 2^2 = 4$ in.^{2}

$r^2 = (1.9)^2 = 3.61$ in.^{2}

$A = \pi(0.39) = 1.225$ in.^{2}

$\therefore$ the stress due to axial loads is:

$$\sigma_{axial} = \frac{P}{A} = \frac{P}{1.225} = 0.8155\ P \text{ (psi)}.$$

The combined stress is then,

$$\sigma_c = \sigma_{bending} + \sigma_{axial} = 0.8555\ M_R + 0.8155\ P \text{ (psi)},$$

where the bending and axial stress are the same sign. Tables VII and VIII list the stresses at each node point for the two trajectories.

TABLE V

Moments Due to External Loads for the Orbital Decay Condition

① Time	② N'_Y	③ $\ddot{\alpha}$	④ 7.1725 N'_Y	⑤ 0.04849 $\ddot{\alpha}$	⑥ P_1 = ④ - ⑤	M_{N4} = 8.3 x ⑥	M_{N5} = 10.3 x ⑥	M_{N6} = 12.3 x ⑥	M_{N7} = 14.3 x ⑥
1650	0.846	35.1	6.072	1.702	4.370	36.3	45.0	53.8	62.5
1700	1.037	77.1	7.443	3.739	3.704	30.7	38.2	45.6	53.0
1725	1.908	128.4	13.695	6.226	7.469	62.0	76.9	91.9	106.8
1750	2.024	176.1	14.527	8.539	5.988	49.7	61.7	73.7	85.6
1770	1.689	82.5	12.123	4.000	8.123	67.4	83.7	99.9	116.2
1780	1.807	88.4	12.970	4.287	8.683	72.1	89.4	106.8	124.2
1800	1.349	62.6	9.682	3.035	6.647	55.2	68.5	81.8	95.1
1820	0.959	63.9	6.883	3.099	3.784	31.4	39.0	46.5	54.1

TABLE VI

Moments Due to External Loads for the -6.4 Degree Reentry Condition

Time (sec)	① N_Y (g)	② $\ddot{\alpha}$ (rad/sec^2)	③ 0.001052 x ②	④ N'_Y = ① - ③	⑤ 7.1725 x ④	⑥ 0.04849 x ②	⑦ P_1 = ⑤ - ⑥	M_{N4} = 8.3 x ⑦ (in.-lb)	M_{N5} = 10.3 x ⑦ (in.-lb)	M_{N6} = 12.3 x ⑦ (in.-lb)	M_{N7} = 14.3 x ⑦ (in.-lb)
50	0.937	50.535	0.053	0.884	6.340	2.450	3.890	32.287	40.067	47.847	55.627
55	1.220	51.600	0.054	1.167	8.370	2.502	5.868	48.704	60.440	72.176	83.912
58	1.256	44.939	0.047	1.209	8.672	2.179	6.493	53.892	66.878	79.864	92.850
63	1.548	48.544	0.051	1.497	10.608	2.354	8.254	68.508	85.016	101.52	118.032
66	1.787	51.949	0.055	1.732	12.423	2.519	9.904	82.203	102.011	121.819	141.627
70	2.174	63.343	0.067	2.107	15.112	3.072	12.040	99.932	124.012	148.092	172.172
75	2.579	63.272	0.067	2.512	18.017	3.068	14.949	124.077	153.975	183.873	213.771
77	2.717	66.776	0.070	2.647	18.986	3.238	15.748	130.708	162.204	193.700	225.196
80	2.791	68.711	0.072	2.719	19.502	3.332	16.170	134.211	166.551	198.891	231.231

TABLE VII

Resultant Stresses at Nodes 4, 5, 6, and 7
For the Orbital Decay Condition

Time	① M_1	② M_N	③ $M_R = \lvert ① - ② \rvert$	④ A	⑤ 0.816 x ④	⑥ 0.858 x ③	σ = ⑤ + ⑥
				Node 4			
1650	43	36	7	10	8	6	14
1700	51	31	20	27	22	17	39
1725	97	62	35	48	39	30	69
1750	104	50	54	77	63	46	109
1770	84	67	17	106	86	15	101
1780	91	72	19	113	92	16	108
1800	67	55	12	78	64	10	74
1820	49	31	18	45	37	15	52
				Node 5			
1650	46	45	1	10	8	1	9
1700	56	38	16	27	22	14	36
1725	105	77	28	47	38	24	62
1750	116	62	54	76	62	46	108
1770	90	84	6	105	86	5	91
1780	97	89	8	112	91	7	98
1800	71	69	2	77	63	2	65
1820	54	39	15	44	36	13	49
				Node 6			
1650	44	54	10	9	7	9	16
1700	56	46	10	26	21	9	30
1725	103	92	11	47	38	9	47
1750	116	74	42	75	61	36	97
1770	87	100	13	104	85	11	96
1780	93	107	14	111	91	12	103
1800	69	82	13	76	62	11	73
1820	53	47	6	44	36	5	41
				Node 7			
1650	37	63	26	9	7	22	29
1700	48	53	5	26	21	4	25
1725	89	107	18	46	38	15	53
1750	101	86	15	74	60	13	73
1770	74	116	42	102	83	36	119
1780	79	124	45	109	89	39	128
1800	59	95	36	75	61	31	92
1820	45	54	9	43	35	8	43

TABLE VIII

Resultant Stresses at Nodes 4, 5, 6, and 7
For the -6.4 Degree Reentry Condition

Time (sec)	M_1 (in.-lb)	M_N (in.-lb)	$\lvert M_R \rvert = M_1 - M_N$	A (lb)	⑤ 0.816 A (psi)	⑥ 0.858 $\lvert M_R \rvert$ (psi)	σ = ⑤ + ⑥ (psi)
			Node Point 4				
50	44	32.3	11.7	41	33.5	10.0	43.5
55	58	48.7	9.3	65	53.0	8.0	61.0
58	59	53.9	5.1	82	66.9	4.4	71.3
63	74	68.5	5.5	114	93.0	4.7	97.7
66	85	82.2	2.8	131	106.9	2.4	109.3
70	103	99.9	3.1	160	130.6	2.7	133.3
75	123	124.1	1.1	192	156.7	0.9	157.6
77	129	130.7	1.7	202	164.8	1.5	166.3
80	133	134.2	1.2	209	170.5	1.0	171.5
			Node Point 5				
50	47	40.0	7.0	41	33.5	6.0	39.5
55	61	60.4	0.6	64	52.2	0.5	52.7
58	62	66.8	4.8	81	66.1	4.1	70.2
63	77	85.0	8.0	112	91.4	6.9	98.3
66	88	102.0	14.0	130	106.1	12.0	118.1
70	107	124.0	17.0	158	128.9	14.6	143.5
75	127	154.0	27.0	190	155.0	23.2	178.2
77	133	162.2	29.2	199	162.4	25.1	187.5
80	137	166.6	29.6	206	168.1	25.4	193.5
			Node Point 6				
50	46	47.8	1.8	40	32.6	1.5	34.1
55	58	72.2	14.2	63	51.4	12.2	63.6
58	59	79.9	20.9	80	65.3	17.9	83.2
63	73	101.5	28.5	111	90.6	24.5	115.1
66	84	121.8	37.8	129	105.3	32.4	137.7
70	101	148.1	47.1	156	127.2	40.4	167.6
75	119	183.9	64.9	188	153.4	55.7	209.1
77	126	193.7	67.7	197	160.7	58.1	218.8
80	129	198.9	69.9	203	165.6	60.0	225.6
			Node Point 7				
50	39	55.6	16.6	40	32.6	14.2	46.8
55	50	83.9	33.9	62	50.6	29.1	79.7
58	50	92.9	42.9	80	65.3	36.8	102.1
63	61	118.0	57.0	110	89.8	48.9	138.7
66	70	141.6	71.6	127	103.6	61.4	165.0
70	85	172.2	87.2	155	126.4	74.8	201.2
75	100	213.8	113.8	185	151.0	97.6	249.6
77	105	225.2	120.2	198	161.6	103.1	264.7
80	108	231.2	123.2	201	164.0	105.7	269.7

Figures 10 through 13 show the relationship between temperature and maximum combined stress for node points 4, 5, 6, and 7 for the orbital decay condition. Plotted in these same figures is the interpolated relationship between yield stress and temperature for beryllium. The arrows on the curves indicate an increase in time. Likewise, Figures 14 through 17 show the corresponding relationship for the -6.4 degree reentry condition.

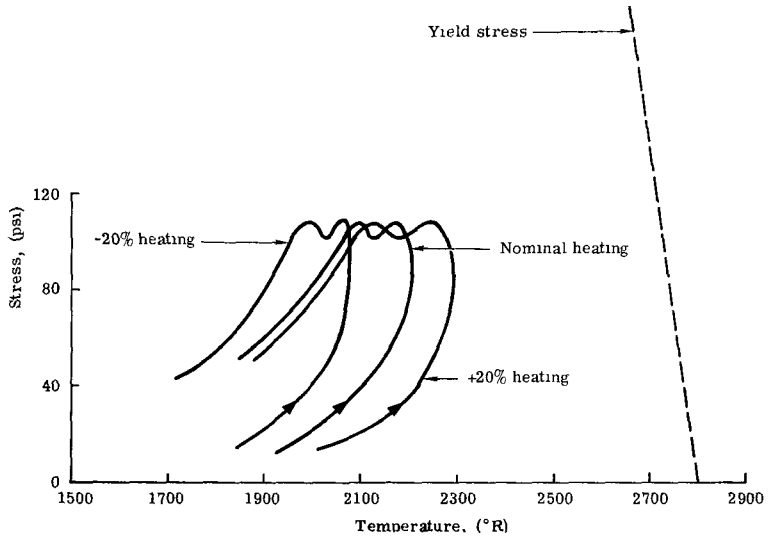

Figure 10.

Stress vs temperature at Node 4 for the orbital decay condition

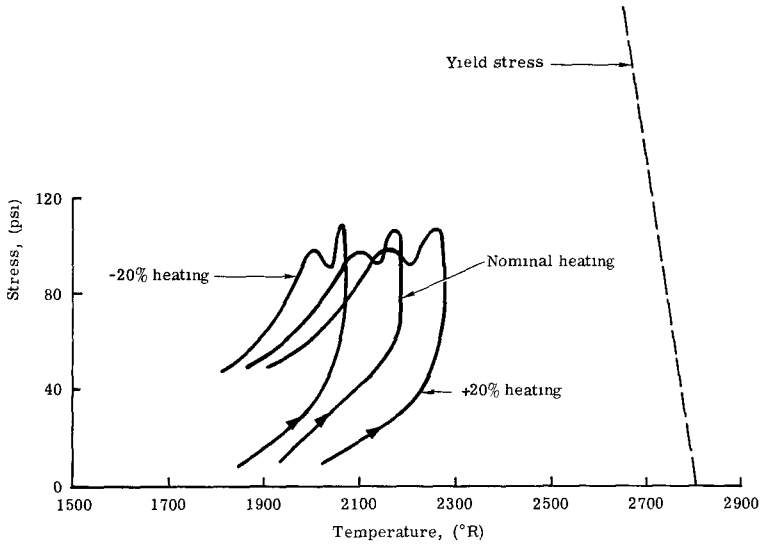

Figure 11.

Stress vs temperature at Node 5 for the orbital decay condition

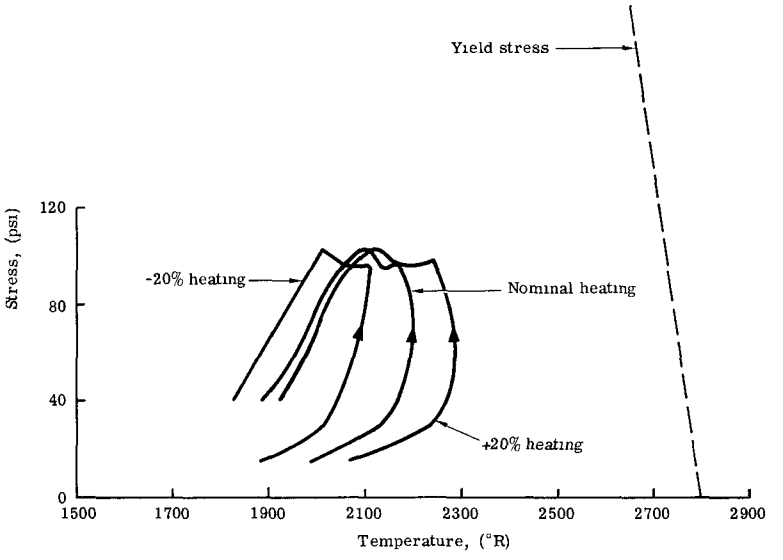

Figure 12. Stress vs temperature at Node 6 for the orbital decay condition

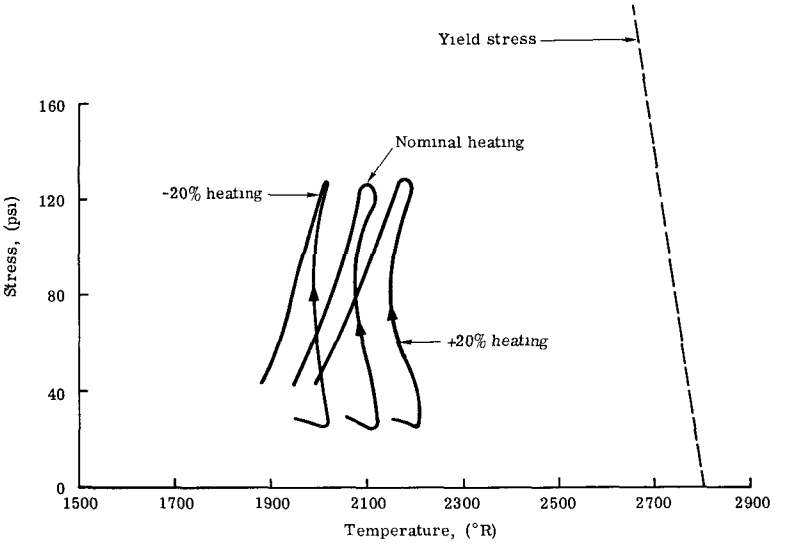

Figure 13. Stress vs temperature at Node 7 for the orbital decay condition

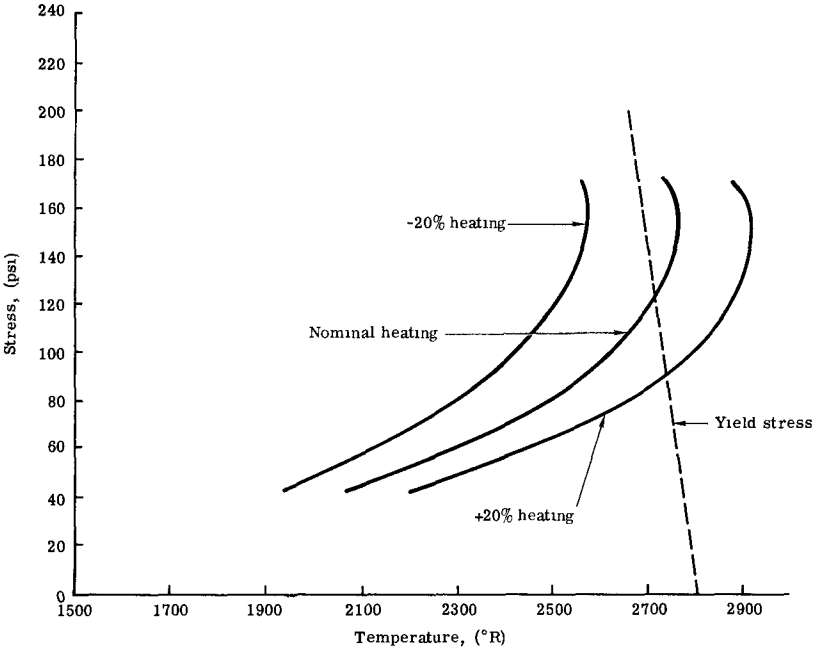

Figure 14. Stress vs temperature at Node 4 for the -6.4 degree reentry condition

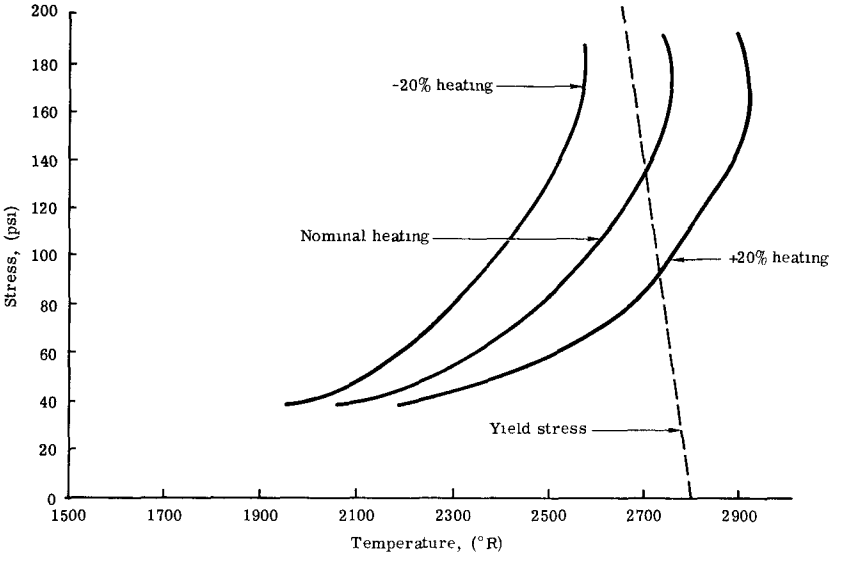

Figure 15. Stress vs temperature at Node 5 for the -6.4 degree reentry condition

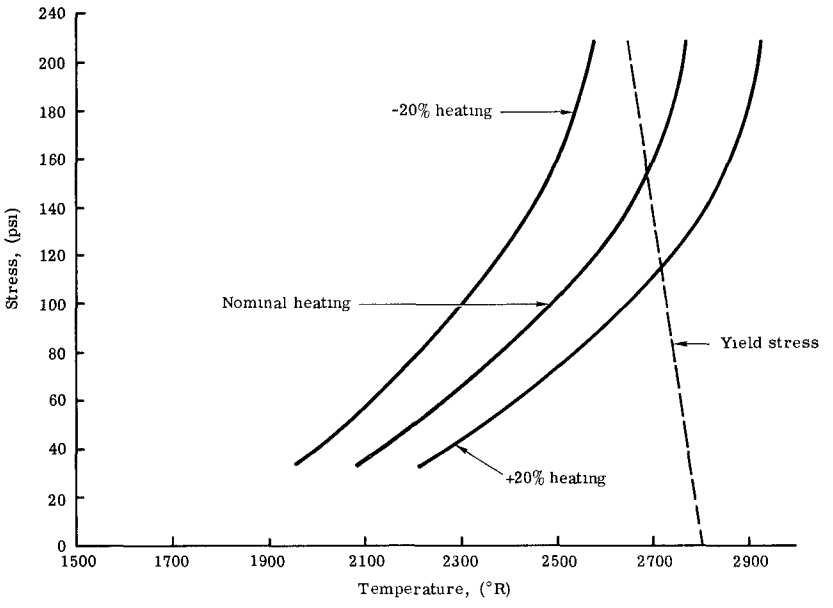

Figure 16. Stress vs temperature at Node 6 for the -6.4 degree reentry condition

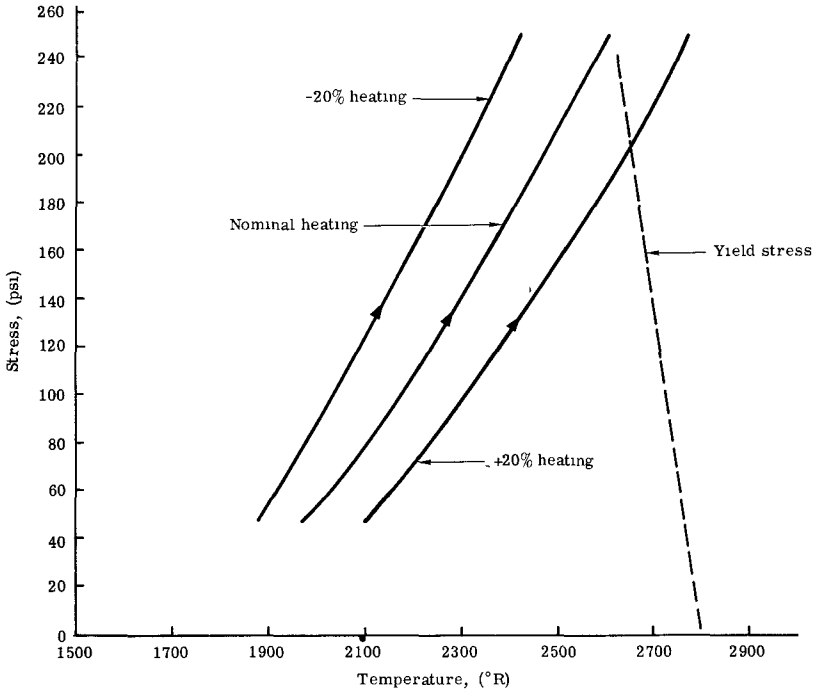

Figure 17. Stress vs temperature at Node 7 for the -6.4 degree reentry condition

Orbital Decay Condition

The stress-temperature curves for each of the nodes for all three heating rates lie to the left of the yield stress line. Given the possibility, as mentioned before, that the actual yield stress curve could lie below the one shown, it would still appear that yielding of the beryllium cylinder is not likely. Therefore, the orbital decay trajectory should not cause any structural problems.

-6.4 Degree Reentry Trajectory

The stress-temperature curves for this condition intersect the yield stress line under the nominal and +20 percent heating rates for all four node points. Only the -20 percent heating rate lies to the left of the yield line. In the cases of Node 6 and, especially, Node 7, the probability of this line intersecting the yield line appears to be high based on the trend of the stress-temperature curves. Structural damage, then, appears to be probable for the -6.4 degree reentry condition.

-30 Degree Reentry Trajectory

Temperatures for this condition reached the melting point of the beryllium very early in the trajectory and structural failure of the cylinder will occur.

References

1. R. E. Berry, et al, Aerothermodynamic and Structural Analyses of the SNAP-27 Fuel Cask, SC-RR-66-2651, Sandia Corporation, Albuquerque, New Mexico, January 1967.

2. Aerospace Structural Metals Handbook, Vol. II, Syracuse University Press, Syracuse, New York, March 1963.

3. D. R. Yeager, Results of a Wind Tunnel Test Program to Determine the Static Stability, Dynamic Stability and Pressure Distribution for the SNAP-27 Configuration at Mach 6 Through 10, ATDM 66-6, General Electric Co., Missile and Space Division, Valley Forge, Pa., July 21, 1966.

SPECIFIED DISTRIBUTION ONLY

DISTRIBUTION:
U.S. Atomic Energy Commission
Director, Space Nuclear Systems
Space Electric Power Office
Washington, D.C. 20545
Attn: G. P. Dix, Chief
Safety Branch (4)

Administrator National Aeronautics
and Space Administration
Washington, D.C. 20545
Attn: T. B. Kerr (RNS) (3)

National Aeronautics and Space Adm.
Manned Spacecraft Center
Houston, Texas 77058
Attn: W. C. Remini, ZS-5 (1)
J. R. Briley, EP-5 (1)

General Electric Company
Valley Forge Space Tech. Center,
P.O. Box 8555
Philadelphia, Pennsylvania 19101
Attn: T. F. Widmer (3)

V. E. Blake, 9310
S. L. Jeffers, 9312 (2)
S. McAlees, Jr., 9314 (4)
J. D. Appel, 9319
Aerospace Nuclear Safety
Information Center, 9319 (2)
J. W. McKiernan, 9331
B. F. Hefley, 8232
B. R. Allen, 3421
W. K. Cox, 3428-1, Bldg. 802
L. C. Baldwin, 3412 (1)
Attn: L. L. Alpaugh, Jr., 3412 (1)
C. H. Sproul, 3428-2 (10)

REPRODUCTION PERMISSION